

DETECTION OF SURFACE VARIATIONS ON CURVED MIRRORS OF VEHICLES USING SLIGHT DEVIATION CONTROL TECHNIQUES

HONG-DAR LIN AND KUAN-SHEN HSIEH

Department of Industrial Engineering and Management
Chaoyang University of Technology
168, Jifeng E. Rd., Wufeng District, Taichung 41349, Taiwan
hdlin@cyut.edu.tw

Received October 2017; revised March 2018

ABSTRACT. *Curved mirrors have been widely adopted in rearview mirrors of vehicles and security mirrors on driving roads to provide drivers with better viewing fields and driving information. In the manufacturing process of curved mirrors, surface variation flaws can result from unstable temperature changes of ovens and inappropriate control of over-flow fusion process. Flawed car mirrors with surface distortion provide shape-distorted scene information and may thus cause drivers to make wrong decisions when driving. This study proposes a novel vision system based on slight deviation control techniques to detect surface variations on curved mirrors of vehicles. To quantify the deformation of a car mirror, a standard inspection pattern is designed to reflect the pattern on a testing car mirror for image acquisition. The reflected pattern image of a defective mirror with distortion is compared with that of a normal mirror for quantifying the deformation and locating the distortion flaws. We first detect the intersection points of the standard pattern, then measure the distances of the intersection points from the origin, and calculate the distance deviations of the corresponding intersection points between the defective and the normal images. Finally, the slight deviation control techniques, cumulative sum method and exponentially weighted moving average method are applied to judging the existence of the distortion flaws based on the accumulative deviation distances. Experimental results show that the suggested methods achieve a high probability (98%) of correctly discriminating distortion flaws on curved mirrors of vehicles.*

Keywords: Visual inspection system, Curved mirrors of vehicles, Surface variations, Slight deviation control techniques

1. Introduction. Compared with plane mirrors of vehicles, curved mirrors have higher reflectance and wider field of view. Curved mirrors have been widely adopted in rearview mirrors of vehicles and security mirrors on the driving roads to provide drivers with better viewing fields and driving information. In the manufacturing process of curved mirrors of vehicles, surface variation flaws often result from unstable temperature changes of ovens and inappropriate control of over-flow fusion process. Since distortion flaws do not have regular shapes and clear boundaries, it is not easy to measure magnitudes of distortion flaws on curved mirrors. Flawed car mirrors with distortion provide shape-distorted scene information and may thus cause drivers to make wrong decisions when driving. Figure 1 shows the flawless and flawed images of curved mirror surfaces with reflection of street scene. The object shapes reflected in the flawed image are significantly distorted (Figure 1(b)). The mirror distortion flaws can make reflected objects look irregular, out of focus,



FIGURE 1. Curved mirror images of vehicles with reflection of street scene: (a) a flawless image; (b) a flawed image with distortion

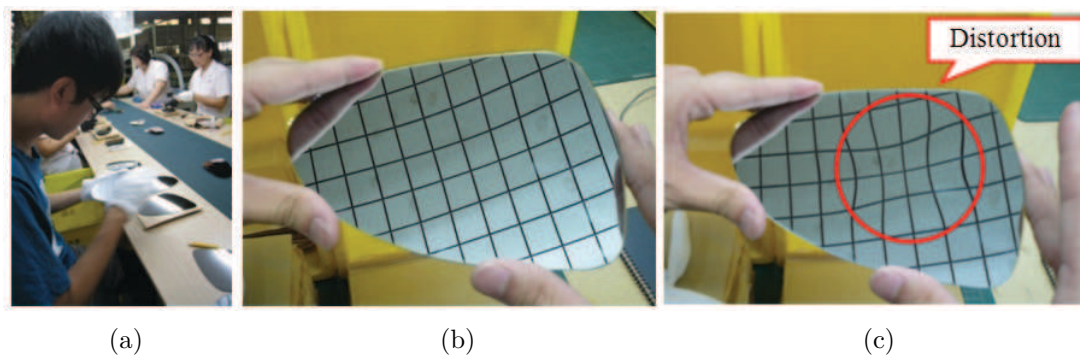


FIGURE 2. (a) Present inspection tasks conducted by human visual judgment; (b) the flawless image and (c) the flawed image with reflection of a standard pattern

and blurry in the flawed images. These distorted images may lead drivers to make wrong judgment and thus cause dangerous car accidents.

Inspection difficulties of surface defects exist in the manufacturing process of curved mirrors. Surface flaws affect not only the appearance of industrial parts but also their functionality, efficiency and stability. The most common detection methods for surface flaws are human visual inspections, which are vulnerable to wrong judgments owing to inspectors' subjectivity and eye fatigues. Figure 2 shows the present inspection tasks conducted by human visual judgment, and the flawless image and the flawed image with reflection of a standard pattern.

Present vision system (off-line and sampling) with a concentric circle pattern and a testing platform (Figure 3) uses the concentric circle pattern reflected on mirrors to acquire images and quantify distortion magnitude for selection. It used only 8 intersection points on the concentric circle pattern to roughly calculate distortion rate. It is hard to accurately inspect the mirror distortion flaws by present vision systems due to high reflection. High reflection on curved mirrors increases the difficulty of discriminating the distortion flaws on car mirrors. In this research, the testing samples with length 18.1cm, width 10.71cm, and thickness 0.2cm, were randomly selected from the manufacturing process of car mirrors. Figure 4 shows the dimension of a testing sample (Figure 4(a)) and a captured image with high reflection on mirror surface (Figure 4(b)). This study proposes a novel vision system with a trapezoidal mask for image acquisition and applies slight deviation control techniques to inspecting distortion flaws on curved mirrors of vehicles.

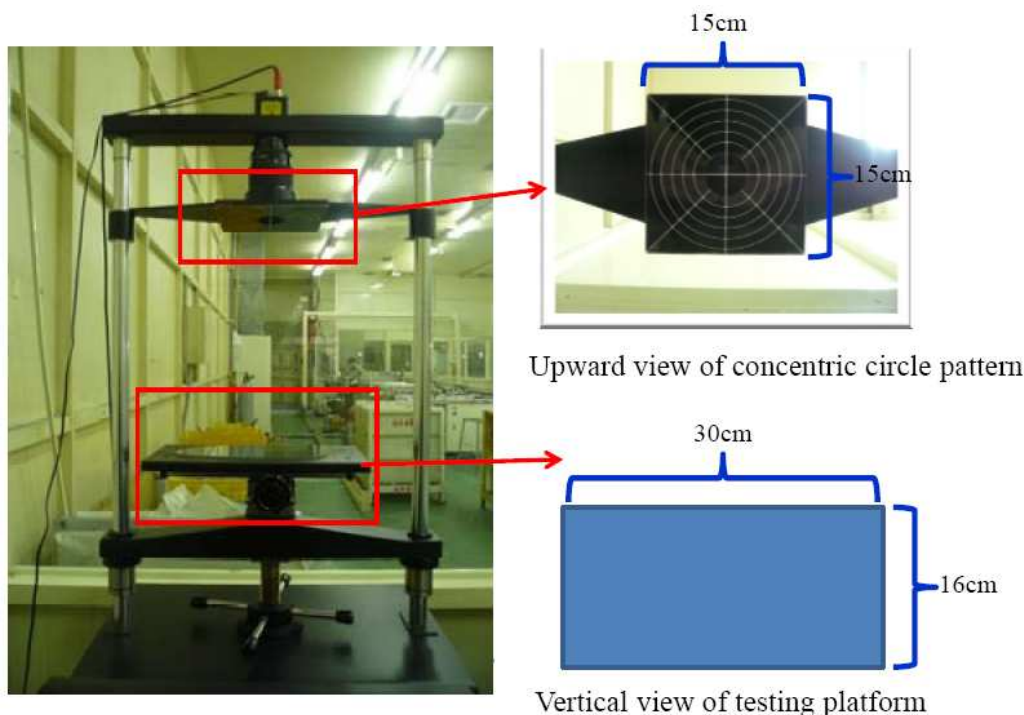


FIGURE 3. Present vision system with a concentric circle pattern (upward view) and a testing platform (vertical view)

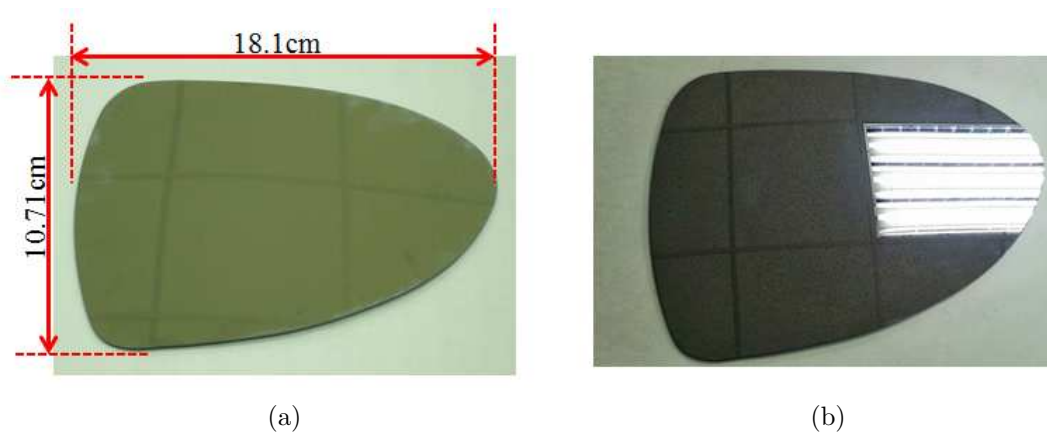


FIGURE 4. (a) Dimension of the testing sample and (b) an acquired image with high reflection

2. Literature Review. Automatic visual inspection of flaws has become a crucial mission for industries which exert to upgrade product quality and manufacturing efficiency [1-3]. Lin and Chiu [4] developed a machine vision system to find mass centers of chips, locate cutting lines and estimate process regulation plans for the automated and high-speed dicing of electronic passive components. Lin and Li [5] developed a wavelet transform-based approach to inspecting the area defects on appearances of touch panels. Adamo et al. [6] proposed a low-cost inspection system based on the Canny edge detection for online defects assessment in satin glass. Liu et al. [7] presented the method based on watershed transform methods to segment the possible defective regions and extract features of bottle wall by rules.

Many studies investigated the flaw inspection of glass related products. Li and Tsai [8] proposed a wavelet-based discriminant measure for defect inspection in multi-crystalline

solar wafer images with inhomogeneous texture. Lin and Tsai [9] presented a Fourier transform-based approach to inspecting surface defects of capacitive touch panels. Chiu and Lin [10] applied block discrete cosine transform, Hotelling's T-squared statistic, and grey clustering technique for the automatic detection of visual blemishes in curved surfaces of LED lenses. These visual inspection systems focus mainly on the surface blemish detection.

In photography, distortion is especially associated with zoom lenses, particularly large-range zooms. Regarding the distortion correction techniques, Duan and Wu [11] proposed a new method for distortion correction in the barrel distortion of wide-angle lens. The cubic B-spline interpolation function was adopted to interpolate the surface and the bilinear interpolation was used to reconstruct the gray level of pixels. Sun et al. [12] presented a piecewise spline function to describe the distortion and obtained a continuous smooth distortion model after eliminating noises using smoothing spline algorithm. Since this method corrected lens distortion on pixel plane, it obtains unbiased displacement in image correlation. Chang et al. [13] addressed super-resolution images with nonlinear lens distortions through deep convolutional neural network with residual learning. This camera calibration method can significantly improve the image quality. Santana-Cedr es et al. [14] developed a novel method for automatic correction of perspective and optical distortions by using lens distortion model and vanishing points. Furnari et al. [15] introduced a set of distortion adaptive Sobel filters for the direct estimation of geometrically correct gradients of wide angle images. This method excels in both gradient estimation and key point matching for images with large amounts of radial distortion. From the above review of literature, it is evident that most of the distortion related works focus on the distortion correction of optical lenses.

In distortion defect inspection studies of industrial parts, Jin et al. [16] presented an inspection method based on phase image processing in grating projection for glass defect detection. Jin et al. [17] suggested a grating projection based method for measuring deformation degree of optical distortion to detect glass defect. The proposed algorithm used one-dimensional Fourier transform and elimination method of edge effect to process the fringe image. Chiu et al. [18] implemented a Hough transform based technique for distortion defect detection on transparent glass. These frequency domain based approaches need more processing time to complete the mathematical transformations.

Currently, the majority of automated inspection systems of mirrors mainly detect surface defects and the distortion flaws are not included. It is hard to accurately detect reflected distortion flaws embedded on surface of curved mirrors of vehicles with high reflection. Presently, very few research studies apply automated visual inspection systems to inspecting mirror distortion flaws. Therefore, we propose a vision system based on slight deviation control techniques to detect reflected distortion flaws on curved mirrors.

3. Suggested Methods. To quantify the deformation of a flawed mirror with surface distortion, this study proposes a standard inspection pattern with checkerboard grids to reflect the pattern on a testing mirror for image acquisition. The reflected pattern image of the surface distorted mirror is compared with that of a normal mirror for measuring the deformation and locating the distortion flaws. Firstly, we detect the intersection points of the standard inspection pattern, then measure distances of the intersection points from the origin, and calculate distance deviations of the corresponding intersection points between the defective and normal images. Finally, we apply the slight deviation control techniques to determining the existence of the distortion flaws based on detecting slight changes of the distance deviations. We describe this procedure in the following subsections in detail.

3.1. Image acquisition. To distinctly acquire images with appropriate reflection for image processing, this study suggests a vision system with a trapezoidal mask for image acquisition shown in Figure 5. A testing sample is placed on bottom of the mask and a standard checkerboard pattern is attached on the top inside the mask. The proposed vision system uses the checkerboard pattern reflected on mirrors to capture images and quantify distortion magnitude for slight deviation control. Figure 6 shows three-view drawings of the trapezoid mask and specifications of the standard pattern. Dimensions of the trapezoidal mask are described on the three-view drawings (Figure 6(a)). The circle on the central part of the top view drawing is used to fix the camera lens. The central

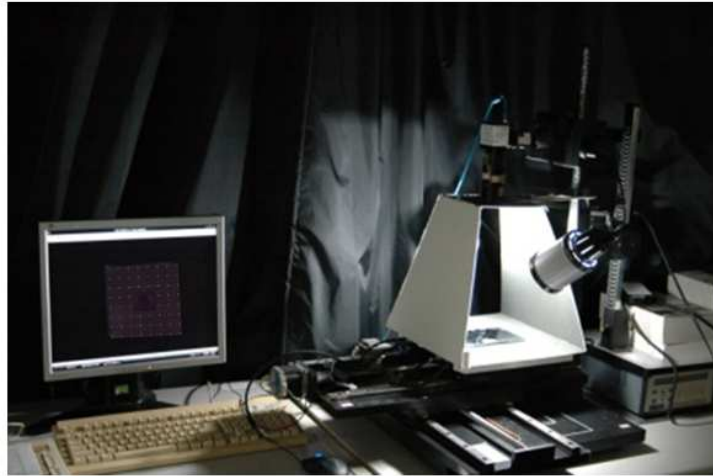


FIGURE 5. Structures of the exploratory circumstance where scanning a trial mirror sample

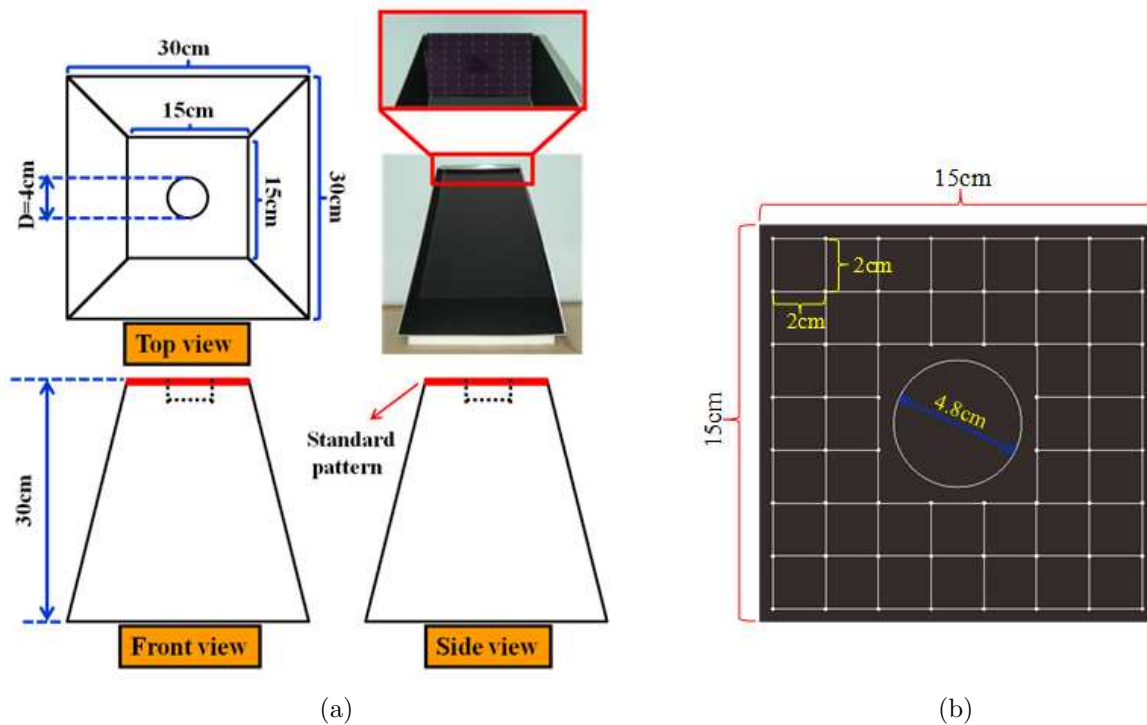


FIGURE 6. (a) Three-view drawings of the trapezoid mask; (b) specifications of the standard checkerboard pattern

circle region of the checkerboard pattern (Figure 6(b)) is the undetected area because the corresponding region on a testing mirror reflects the camera lens. To clearly capture images with suitable reflected intensity, the control of lighting source in exploratory environment is very important. Figure 7 demonstrates outcomes of the proposed image acquisition environment using trapezoidal mask and light source: (a) a captured image without suitable light source; (b) a captured image with appropriate light source. After a clear image has been captured, the image has to be processed which involves segmentation, feature extraction, and slight deviation control.

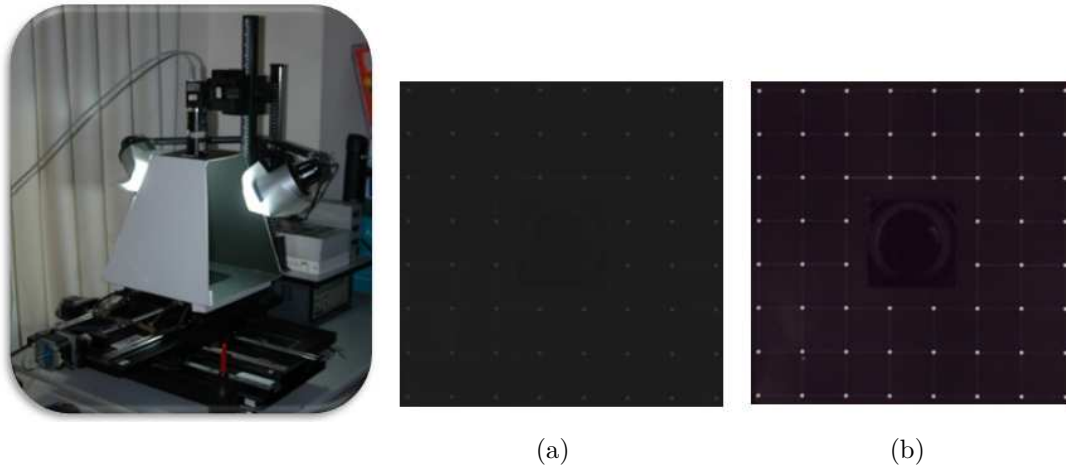


FIGURE 7. Outcomes of image acquisition with trapezoidal mask and light source: (a) a captured image without suitable light source; (b) a captured image with proper light source

3.2. Image processing procedures. To measure deformation of mirror images, the captured testing images have to be processed in several steps. Figure 8 illustrates the procedure of image processing and outcomes performed by the suggested approach for detecting distortion flaws on curved mirror images. Figures 8(a) and 8(b) represent the captured testing image and the corresponding gray level image using the checkerboard pattern. Figure 8(c) depicts the binary image that the Otsu method [19] applied to doing segmentation. Figure 8(d) describes the feature extraction of the feature points in the checkerboard pattern and applies the slight deviation control techniques (CUSUM method and EWMA method). And, Figure 8(e) presents the resulting image showing the detected distortion flaws (marked in gray dots and mesh on lower half) by the suggested detection method. The results reveal that the slight distortion flaws on curved mirror surface are correctly separated in a binary image, regardless of insignificant distortion magnitudes. We introduce the two standard patterns, concentric circle pattern and checkerboard pattern, in Subsections 3.4 and 3.5 and the two slight deviation control techniques in Subsections 3.6 and 3.7.

3.3. Standard concentric circle pattern. A standard concentric circle pattern includes 6 concentric circles and 4 axes dividing a cycle into equal 8 parts in this study. Figure 9(a) shows intersection points and notations between the circles and lines in the concentric circle pattern and Figure 9(b) illustrates coordinate notations of 8 intersection points on the innermost concentric circle. For each of the 6 concentric circles, it includes 8 intersection points $I_{i,j}$ (feature points) with coordinates $(x_{i,j}, y_{i,j})$ and 8 distances $d_{i,j}$ (feature values) between the intersection points and center point of the concentric circles.

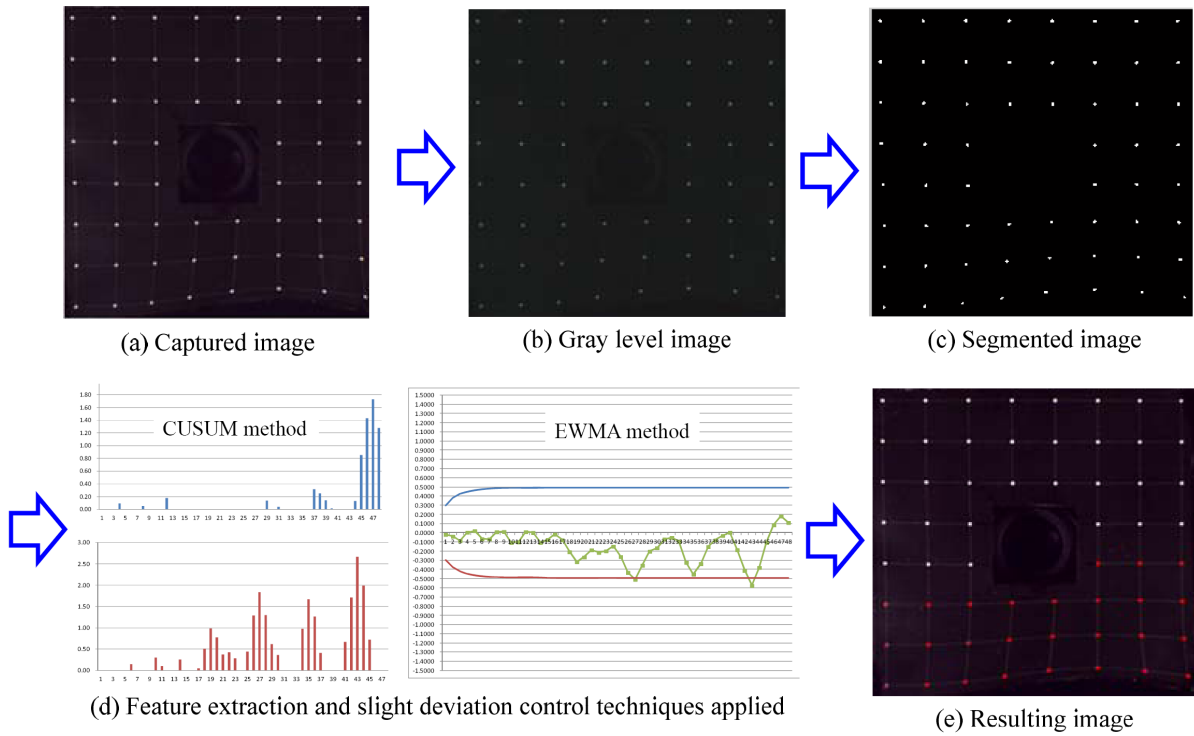


FIGURE 8. The image processing procedure of the suggested methods

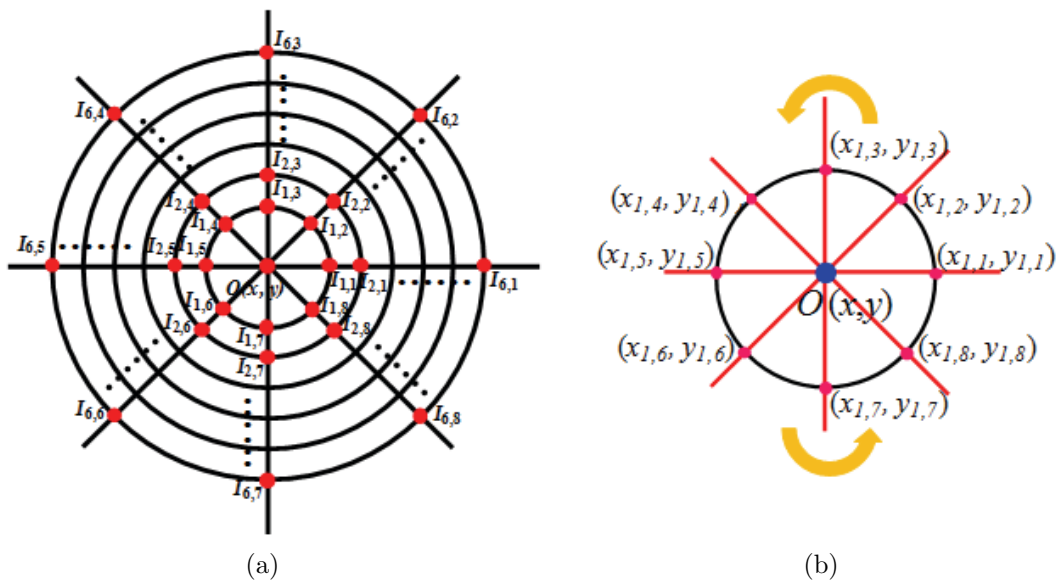


FIGURE 9. (a) Intersection points and notations in the concentric circle pattern; (b) coordinate notations of 8 intersection points on the innermost concentric circle

The center point $O(x, y)$ is determined by the 8 intersection points of the innermost circle:

$$O(x, y) = \left(\frac{1}{m \times n} \sum_{i=1}^m \sum_{j=1}^n x_{i,j}, \frac{1}{m \times n} \sum_{i=1}^m \sum_{j=1}^n y_{i,j} \right) \quad (1)$$

where $m = 1, n = 8$. And, the feature values $d_{i,j}$ are the distances calculated from $O(x, y)$ and $I_{i,j}(x_{i,j}, y_{i,j})$, correspondingly:

$$d_{i,j} = \sqrt{(x_{i,j} - x)^2 + (y_{i,j} - y)^2} \tag{2}$$

Feature values of the concentric circle pattern in a testing image will be compared with those of a normal image to measure the deviations of the corresponding distances for locating the distortion flaws on testing images.

3.4. Standard checkerboard grid pattern. A standard checkerboard grid pattern includes 3 concentric squares and several vertical and horizontal line segments dividing the 3 squares into equal 40 grids in this study. Figure 10(a) shows intersection points and notations between the squares and lines in the checkerboard grid pattern and Figure 10(b) illustrates coordinate notations of 12 intersection points on the innermost concentric square. For all of the 3 concentric squares, they include 60 intersection points $I_{i,j}$ (feature points) with coordinates $(x_{i,j}, y_{i,j})$ and 60 distances $d_{i,j}$ (feature values) between the intersection points and center point $O(x, y)$ of the concentric squares. The center point $O(x, y)$ is determined by 12 intersection points of the innermost square:

$$O(x, y) = \left(\frac{1}{m \times n} \sum_{i=1}^m \sum_{j=1}^n x_{i,j}, \frac{1}{m \times n} \sum_{i=1}^m \sum_{j=1}^n y_{i,j} \right) \tag{3}$$

where $m = 1, n = 12$. The feature values $d_{i,j}$ are the distances calculated from $O(x, y)$ and $I_{i,j}(x_{i,j}, y_{i,j})$, correspondingly:

$$d_{i,j}(x_{i,j}, y_{i,j}) = \max(|x - x_{i,j}|, |y - y_{i,j}|) \tag{4}$$

Similarly, feature values of the checkerboard pattern in a testing image will be compared with those of a normal image to measure the deviations of the corresponding distances for locating the distortion flaws on testing images.

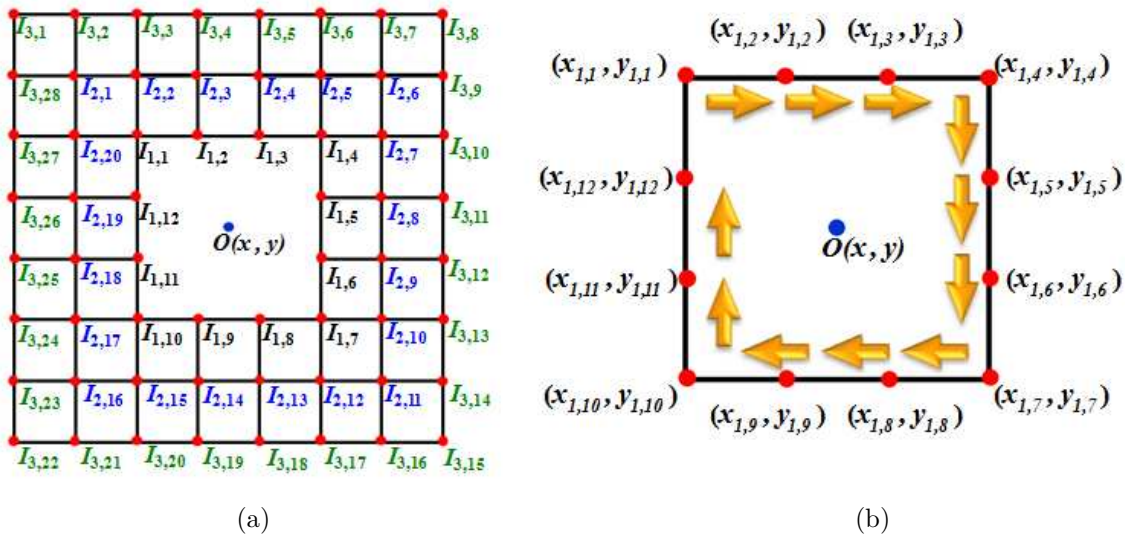


FIGURE 10. (a) Intersection points and notations in the checkerboard grid pattern; (b) coordinate notations of 12 intersection points on the innermost concentric square

3.5. Slight deviation control techniques – CUSUM methods. We measure distances of the intersection points from the origin, and further calculate the distance deviations $\Delta d_{i,j}$ ($\Delta d_{i,j} = d_{i,j} - \overline{d_{i,j}}$) of the corresponding distances of the intersection points between testing image ($d_{i,j}$) and normal image ($\overline{d_{i,j}}$). The slight deviation control techniques are applied to finding slight changes of the distance deviations for detecting distortion flaws.

3.5.1. Tabular cumulative sum (CUSUM) approach. To detect slight changes in the distance deviations, this research suggests the CUSUM algorithm, which is frequently applied in statistical process control to detecting the slight shift or deviation from the normal production process [20,21]. Normally, the CUSUM method processes data, which are smooth in the beginning periods and deviate slightly in the later periods [22]. The tabular CUSUM scheme works by accumulating derivations from μ_0 that are above target with one statistic C_s^+ and accumulating derivations from μ_0 that are below target with another statistic C_s^- . The statistics C_s^+ and C_s^- are called one-sided upper and lower cumulative sums, respectively. They are computed as follows:

$$\begin{aligned} C_i^+ &= \max [0, \Delta d_{i,j} - (\mu_0 + K) + C_{i-1}^+] \\ C_i^- &= \max [0, (\mu_0 - K) - \Delta d_{i,j} + C_{i-1}^-] \end{aligned} \tag{5}$$

where $C_0^+ = C_0^- = 0$, $K = \frac{\delta}{2}\sigma$.

In Equation (5), K is usually called the reference value, and it is often chosen about halfway between the target μ_0 and the out-of-control value of the mean μ_1 that we are interested in detecting quickly. Therefore, if the shift is expressed in standard deviation units as $\mu_1 = \mu_0 + \delta\sigma$, then K is half the magnitude of the shift.

$$K = \frac{\delta}{2}\sigma = \frac{|\mu_1 - \mu_0|}{2} \Rightarrow \delta\sigma = |\mu_1 - \mu_0| \Rightarrow \delta = \frac{|\mu_1 - \mu_0|}{\sigma} \tag{6}$$

Note that C_s^+ and C_s^- accumulate deviations from the target value μ_0 that are greater than K , with both quantities reset to zero on becoming negative. When either C_s^+ or C_s^- exceeds the decision interval H , the sample set is considered to be out-of-control. A reasonable value for H is five times the standard deviation σ [23].

3.5.2. Standardized CUSUM approach. Two advantages of the standardized CUSUM scheme are that the choices of the parameters k and h do not depend on standard deviation, and the other is that the standardized CUSUM scheme leads naturally to a cumulative sum for controlling variability [23]. The standardized cumulative sums are defined as:

$$\begin{aligned} y_i &= \frac{x_i - \mu_0}{\sigma}, \\ C_i^+ &= \max [0, y_i - k + C_{i-1}^+], \quad C_i^- = \max [0, -k - y_i + C_{i-1}^-] \end{aligned} \tag{7}$$

where the initial values $C_i^+ = C_i^- = 0$, $i = 0$.

3.6. Slight deviation control techniques – EWMA method. The exponentially weighted moving average (EWMA) control method is also a good alternative in detecting slight deviations [23-25]. The exponentially weighted moving average Z_i is defined as:

$$Z_i = \lambda x_i + (1 - \lambda)Z_{i-1} \tag{8}$$

where $0 < \lambda \leq 1$ is a constant and the starting value is the process target $Z_0 = \mu_0$. The values of the parameter λ smoothing constant or called weight in the interval $0.05 \sim 0.25$ work well for small shift detection in practice. A general guideline is to use smaller value

of λ to detect smaller shifts. The control limits for the EWMA control method are as follows:

$$\begin{aligned} UCL_i &= \bar{X} + L\sigma\sqrt{\frac{\lambda}{2-\lambda}[1-(1-\lambda^{2i})]} \\ LCL_i &= \bar{X} - L\sigma\sqrt{\frac{\lambda}{2-\lambda}[1-(1-\lambda^{2i})]} \end{aligned} \quad (9)$$

The design parameters of the chart are the multiple of sigma used in the control limits (L) and the value of λ . The performance of the EWMA control technique is approximately equivalent to that of the CUSUM method, and in some ways it is easier to set up and operate [26].

4. Experiments and Results. To assess the effect of the suggested methods, assessments were carried out on actual curved mirrors of vehicles, supplied by a car mirror production plant. All trial samples were arbitrarily chosen from the production process of car mirrors. Testing images (386) of the curved mirrors of vehicles, of which 136 have no flaws and 250 have diverse surface distortion flaws, were examined in our assessments. All images of the mirror appearance have the same size of 256×256 pixels and an intensity of 8 bits. The suggested mirror distortion flaw detection arithmetic is implemented on a personal computer (CPU Core 2 Duo 2.33 GHz and 2GB D-RAM) by MATLAB language (7ed.).

To numerically confirm the manifestation of the suggested method, we contrast the outcomes of our assessments contrary to those supplied by technical assessors (i.e., the ground truth). Three impartial measures: correct classification rate (CCR) and incorrect classification rates (α and β) were assessed for the effect of the distortion flaw detection methods. Statistical type I error (α) measures a probability of generating erroneous alerts, which judge regular areas as flaws. The area of regular regions judged as distortion flaws is divided by the area of real regular regions to gain type I error. Statistical type II error (β) measures a probability of generating lost alerts, which is invalid to alert actual flaws. The area of undetected distortion flaws is divided by the area of real distortion flaws to gain type II error. The higher the effect assessment measures ($1 - \alpha$), ($1 - \beta$), and CCR are, the more exact the detection outcomes are. The correct classification rate CCR is denoted as:

$$CCR = (C_{(1-\alpha)} + C_{(1-\beta)}) / C_{total} \times 100\% \quad (10)$$

where $C_{(1-\alpha)}$ is the pixel number of regular regions correctly detected as flaw-free areas, $C_{(1-\beta)}$ is the pixel number of actual flaw regions right detected as flaw areas, and C_{total} is the pixel number of a testing image.

4.1. ROC curves of performance assessment. If a decisive thresholding changes, two paired measures, erroneous alert rate (α) and detection rate ($1 - \beta$), describing the outcomes of a hypothesis testing will vary [27]. When different thresholding are applied, the sets of erroneous alert rates and detection rates are figured as points in a receiver operating characteristic (ROC) curve. The upper-left corner on an ROC figure represents an ideal outcome having 100% detection rate and a 0% erroneous alert rate. The more the ROC curve moves toward the upper-left corner, the better the trial executes. In manufacturing application, an over 90% detection rate and a below 10% erroneous alert rate are a general guideline for effect assessment of an optical inspection system.

The tabular CUSUM is devised by selecting values for the reference value K and the decision interval H . It is suggested that these parameters be chosen to offer average run length (ARL) performance [23,26]. We define $K = k\sigma$ and $H = h\sigma$, where σ is the

standard deviation of the sample used in establishing the CUSUM. Thus, selections of the parameters k and h decide control limits of the CUSUM methods. Normally, we want to choose k relative to the size of the deviation we want to detect; that is $k = \delta/2$, where δ is the size of the deviation in standard deviation units. In this study, using $h = 4 \sim 5$ and $k = 1 \sim 2.5$ generally provides a CUSUM that has good ARL properties against a deviation of about $1\sigma \sim 2\sigma$ in the process mean.

Table 1 displays the parameter selections and performance assessment of the two CUSUM approaches. Figure 11 illustrates ROC curve of the suggested CUSUM methods with different parameter settings of k and h values, respectively. It indicates the distortion detection performance of the standardized CUSUM approach with parameter settings (k, h) values of $(1.5, 5)$, $(1.5, 5.2)$, or $(1.75, 4)$ is better than those of the Tabular CUSUM approach with parameter settings (k, h) values of $(2.25, 4.6)$ or $(2.25, 4.8)$. Similarly, choices of the parameters λ and L determine control limits of the EWMA method. Figure 12 represents ROC curve of the suggested EWMA method with distinct parameter settings of λ and L values, respectively. It reveals the distortion detection performance of the EWMA method with parameter settings (λ, L) values of $(0.8, 4)$ has the best detection result with erroneous alert rate 4.41% and defect detection rate 98%. Therefore, a suitable method and good parameter selection, with its ROC curve closest to the upper-left corner, defeats the other schemes. This indicates that the more exact parameter settings of the slight deviation detection techniques are chosen, the better outcomes of the distortion detection will have.

TABLE 1. Parameter selections and performance assessment of the two CUSUM methods

Performance Evaluation	Tabular CUSUM	Standardized CUSUM
Erroneous alert rate (α)	5.88%	5.88%
Distortion detection rate ($1 - \beta$)	95.60%	98.00%
Parameters	$k = 2.25$ $h = 4.6, 4.8$	$k = 1.5, h = 5, 5.2$ & $k = 1.75, h = 4$

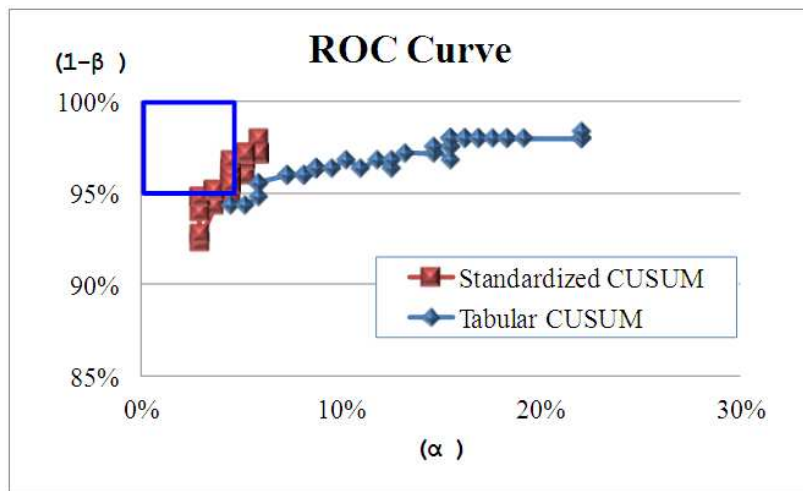


FIGURE 11. Two ROC curves of different cumulative sum approaches

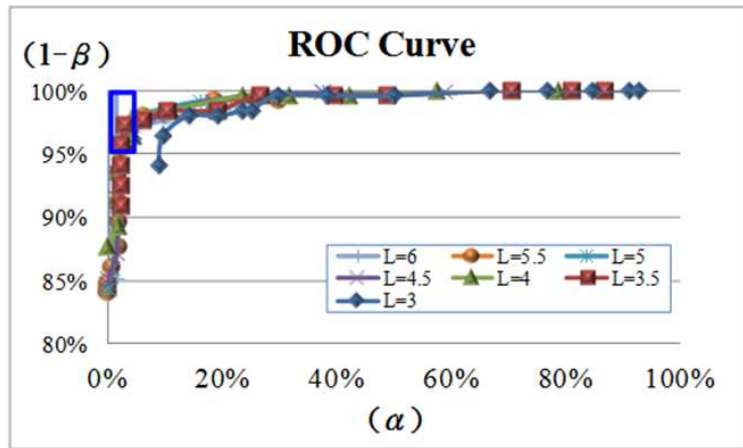


FIGURE 12. Different ROC curves of EWMA method with distinct parameter settings

4.2. **Present visual inspection scheme.** Present visual inspection scheme applies a concentric circle pattern as a typical one to quantifying grades of distortion severity on curved mirrors of vehicles. For the concentric circle pattern, distortion rate $\varepsilon\%$ is computed as:

$$\varepsilon\% = \frac{|d_{i,j} - \bar{d}_i|}{\bar{d}_i} \times 100\% \tag{11}$$

where $d_{i,j}$ is a distance between an intersection point $I(i, j)$ and the center point $O(x, y)$, \bar{d}_i is the average of distances of 8 intersection points on the same concentric circle i , i.e.,

$$\bar{d}_i = \frac{d_{i,1} + d_{i,2} + \dots + d_{i,8}}{8} \tag{12}$$

For a defect-free curved mirror, the distortion rate $\varepsilon\% \leq 3.8\%$. And, for a regular plane mirror, the distortion rate $\varepsilon\% \leq 1.7\%$. If a distortion rate of a testing curved mirror image is more than 3.8%, we can conclude that some distortion flaws exist in the testing image. Table 2 shows parameter settings and performance assessment of the present visual inspection scheme and Figure 13 presents its corresponding ROC curve. The present scheme achieves a better detection outcome with erroneous alert rate 4.41% and distortion detection rate 98% while the threshold of distortion rate 1.15 is used.

4.3. **Performance assessment of distinct detection techniques.** To assess performance of the distortion flaw detection on curved mirrors, Table 3 summarizes the detection outcomes of our tests. Three slight deviation detection methods and two traditional schemes are assessed against the outcomes by professional inspectors. The average distortion detection rates $(1 - \beta)$ of all testing samples by the five methods are 95.6% (Tabular

TABLE 2. Parameter selections and performance assessment of present inspection scheme

Control limits	1	1.05	1.1	1.15	1.2
α	8.09%	8.09%	5.15%	4.41%	2.94%
$(1 - \beta)$	93.20%	92.40%	90.80%	90.80%	88.40%
Control limits	1.25	1.3	1.35	2.5	3.8
α	2.21%	2.21%	2.21%	0.00%	0.00%
$(1 - \beta)$	84.40%	82.40%	81.60%	39.20%	31.60%

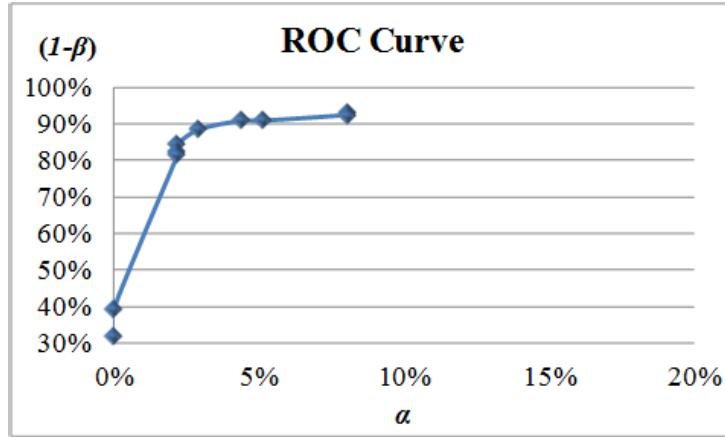


FIGURE 13. The ROC curve of present visual inspection scheme

TABLE 3. Assessment table of distortion flaw detection by five distinct techniques

Methods	Tabular CUSUM ($k = 2.25/h = 4.6, 4.8$)	Standardized CUSUM ($k = 1.75/h = 4$)	EWMA ($\lambda = 0.8, L = 4$)	Shewhart ($L = 4$)	Current visual inspection system (Distortion rate)
α	5.88%	5.88%	4.41%	3.20%	4.41%
$(1 - \beta)$	95.60%	98.00%	98.00%	95.55%	90.80%
Time (sec.)	2.1005	2.1324	1.9724	1.4642	1.1006

CUSUM approach), 98.0% (Standardized CUSUM approach), 98.0% (EWMA method), 95.55% (Shewhart method) [23], and 90.8% (present vision scheme), respectively. Nevertheless, the two cumulative sum approaches have briefly higher erroneous alert rate (α), 5.88% (two CUSUM approaches). Otherwise, the other slight deviation detection method has fairly lower erroneous alert rate, 4.41% (EWMA method). The suggested EWMA method has higher correct classification rates (CCR) than the other techniques applied to distortion flaw detection on curved mirror images. The average processing time for an image with size 256×256 pixels is as follows: 2.10 sec. by Tabular CUSUM approach, 2.13 sec. by Standardized CUSUM approach, 1.97 sec. by EWMA method, 1.46 sec. by Shewhart method, and 1.10 sec. by the present scheme. Hence, the suggested EWMA method conquers difficulties of detecting distortion flaws on curved mirror and surpasses in its ability of accurately differentiating small distortion flaws from regular regions.

The two standard inspection patterns have different detection area coverages: 62.83% for concentric circle pattern and 81.53% for checkerboard pattern. Figure 14 shows the diagrams of undetected areas in the standard inspection patterns. If we use the checkerboard pattern as the standard pattern, there will be more area to be inspected for each testing image. Moreover, the distances between each intersection point and the center point are important feature values to measure the magnitude of mirror distortion flaw. The two standard patterns also have different numbers of the total intersection points per image: 48 points for the concentric circle pattern and 60 points for the checkerboard pattern. The larger the number of intersection points is, the more feature values we will have to more accurately measure the magnitude of distortion flaws. Different total number of the intersection points may result in different detection results for the detection methods. Table 4 summarizes the detection outcomes of the two slight deviation detection methods using the two standard patterns. It indicates that the two slight deviation detection

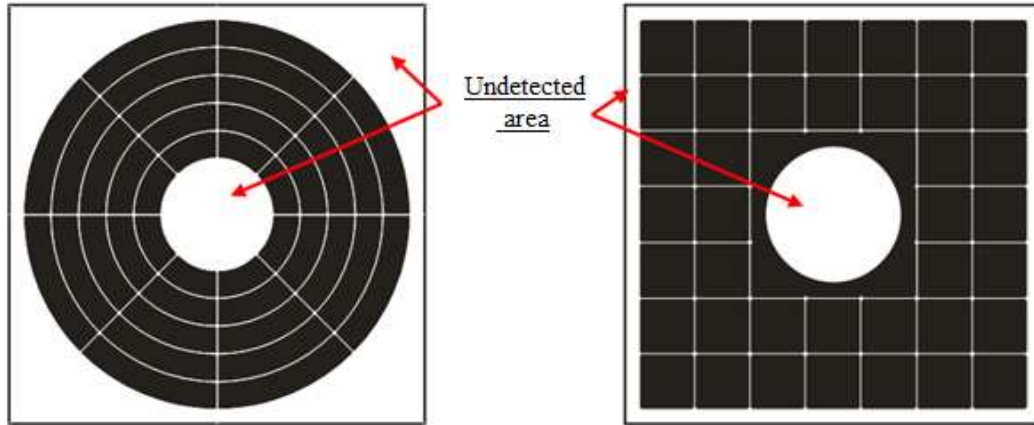


FIGURE 14. Two diagrams of undetected areas in two standard patterns

TABLE 4. Performance assessment of applying two standard patterns to two slight deviation detection methods

Performance Evaluation	Standardized CUSUM		EWMA	
	Checkerboard	Concentric	Checkerboard	Concentric
α	5%	10%	5%	10%
$(1 - \beta)$	96.92%	73.36%	95.38%	90.91%

methods using the checkerboard pattern have better detection performance than those of using the concentric circle pattern.

5. Conclusions. This research proposes a novel vision system based on slight deviation control techniques to inspect surface distortion flaws on curved mirrors of vehicles. To quantify the deformation of a flawed mirror with surface distortion, a standard checkerboard pattern is designed to reflect the pattern on a testing mirror for image acquisition. The reflected pattern image of the surface distorted mirror is compared with that of a regular mirror for measuring the deformation and locating the distortion flaws by the slight deviation control techniques. Experimental outcomes demonstrate that the suggested EWMA method achieves a high probability (98%) of accurately differentiating distortion flaws and a low probability (4.4%) of mistakenly detecting regular images as flawed ones on curved mirror images. Future research may extend the suggested approach to determining the severity levels of the surface distortion flaws (e.g., very serious, serious, moderately serious, and minor) and employ the suggested techniques to detect transparent glass with distinct surface distortion flaws.

Acknowledgment. The authors thank the Ministry of Science and Technology, Taiwan, for the financial support through the Grant MOST 103-2221-E-324-036.

REFERENCES

- [1] J. Liu, Z. Tang, J. Zhang, Q. Chen, P. Xu and W. Liu, Visual perception-based statistical modeling of complex grain image for product quality monitoring and supervision on assembly production line, *PLoS ONE*, vol.11, no.3, 2016.
- [2] L. Q. Liang, D. Li, X. Fu and W. J. Zhang, Touch screen defect inspection based on sparse representation in low resolution images, *Multimedia Tools and Applications*, vol.75, no.5, pp.2655-2666, 2016.

- [3] H.-D. Lin, Y.-S. P. Chiu and W.-T. Lin, An innovative approach for detection of slight surface variations on capacitor chips, *International Journal of Innovative Computing, Information and Control*, vol.9, no.5, pp.1835-1850, 2013.
- [4] H.-D. Lin and Y.-S. P. Chiu, RBF network and EPC method applied to automated process regulations for passive components dicing, *International Journal of Innovative Computing, Information and Control*, vol.6, no.11, pp.5077-5091, 2010.
- [5] H.-D. Lin and J.-M. Li, An innovative quality system for surface blemish detection of touch panels, *International Journal of Applied Engineering Research*, vol.12, no.21, pp.11523-11531, 2017.
- [6] F. Adamo, F. Attivissimo, A. D. Nisio and M. Savino, A low-cost inspection system for online defects assessment in satin glass, *Measurement*, vol.42, pp.1304-1311, 2009.
- [7] H. Liu, Y. Wang and F. Duan, Glass bottle inspector based on machine vision, *International Journal of Computer Systems Science and Engineering*, vol.3, no.3, pp.162-167, 2008.
- [8] W. C. Li and D. M. Tsai, Wavelet-based defect detection in solar wafer images with inhomogeneous texture, *Pattern Recognition*, vol.45, pp.742-756, 2012.
- [9] H.-D. Lin and H.-H. Tsai, Automated quality inspection of surface defects on touch panels, *Journal of the Chinese Institute of Industrial Engineers*, vol.29, no.5, pp.291-302, 2012.
- [10] Y.-P. Chiu and H.-D. Lin, An innovative blemish detection system for curved LED lenses, *Expert Systems with Applications*, vol.40, no.2, pp.471-479, 2013.
- [11] M. L. Duan and K. X. Wu, New method of correcting barrel distortion on lattice model, *Journal of Computer Applications*, vol.32, no.4, pp.1113-1115, 2012.
- [12] Q. Sun, Y. Hou and J. Chen, Lens distortion correction for improving measurement accuracy of digital image correlation, *Optik – International Journal for Light and Electron Optics*, vol.126, no.21, pp.3153-3157, 2015.
- [13] Q. Chang, K. W. Hung and J. Jiang, Deep learning based image super-resolution for nonlinear lens distortions, *Neurocomputing*, vol.275, no.31, pp.969-982, 2018.
- [14] D. Santana-Cedr s, L. Gomez, M. Alem n-Flores, A. Salgado, J. Esclar n, L. Mazorra and L. Alvarez, Automatic correction of perspective and optical distortions, *Computer Vision and Image Understanding*, vol.161, pp.1-10, 2017.
- [15] A. Furnari, G. M. Farinella, A. R. Bruna and S. Battiato, Distortion adaptive Sobel filters for the gradient estimation of wide angle images, *Journal of Visual Communication and Image Representation*, vol.46, pp.165-175, 2017.
- [16] Y. Jin, Z. Wang, Y. Chen, X. Kong, L. Wang and W. Qiao, Study on inspection method of glass defect based on phase image processing, *Optik – International Journal for Light and Electron Optics*, vol.125, no.19, pp.5846-5849, 2014.
- [17] Y. Jin, Z. Wang, Y. Chen and Z. Wang, The online measurement of optical distortion for glass defect based on the grating projection method, *Optik – International Journal for Light and Electron Optics*, vol.127, no.4, pp.2240-2245, 2016.
- [18] Y. P. Chiu, Y. C. Lo and H. D. Lin, Hough transform based approach for surface distortion flaw detection on transparent glass, *International Journal of Applied Engineering Research*, vol.12, no.19, pp.8150-8159, 2017.
- [19] N. Otsu, A threshold selection method from gray level histogram, *IEEE Trans. Systems, Man and Cybernetics*, vol.9, pp.62-66, 1979.
- [20] E. S. Page, Cumulative sum charts, *Technometrics*, vol.3, pp.1-9, 1961.
- [21] A. F. Bissell, CUSUM techniques for quality control, *Applies Statistics*, vol.18, pp.1-30, 1969.
- [22] J. M. Lucas, Cumulative sum (CUSUM) control schemes, *Communications in Statistics – Theory and Methods*, vol.14, no.11, pp.2689-2704, 1985.
- [23] D. C. Montgomery, *Introduction to Statistical Quality Control*, 6th Edition, John Wiley & Sons, Inc., 2009.
- [24] J. M. Lucas and M. S. Saccucci, Exponentially weighted moving average control schemes: Properties and enhancements, *Technometrics*, vol.32, no.1, pp.1-12, 1990.
- [25] F. J. Yu, Y. Y. Yang, M. J. Wang and Z. Wu, Using EWMA control schemes for monitoring wafer quality in negative, *Microelectronics Reliability*, vol.51, pp.400-405, 2011.
- [26] V. C. Vargas and L. F. D. Lopes, Comparative study of the performance of the CuSum and EWMA control charts, *Computers & Industrial Engineering*, vol.46, no.4, pp.707-724, 2004.
- [27] R. O. Duda, P. E. Hart and D. G. Stork, *Pattern Classification*, 2nd Edition, John Wiley & Sons, NJ, 2000.